# Design of photonic band gap fibers with suppressed higher-order modes: Towards the development of effectively single mode large hollow-core fiber platforms

**Kunimasa Saitoh, Nikolaos John Florous, Tadashi Murao, and Masanori Koshiba**

*Division of Media and Network Technologies, Hokkaido University, Sapporo 060-0814, Japan*
*ksaitoh@ist.hokudai.ac.jp*

**Abstract:** The objective of the present investigation is to propose and theoretically demonstrate the effective suppression of higher-order modes in large-hollow-core photonic band gap fibers (PBGFs), mainly for low-loss data transmission platforms and/or high power delivery systems. The proposed design strategy is based on the index-matching mechanism of central air-core modes with defected outer core modes. By incorporating several air-cores in the cladding of the PBGF with 6-fold symmetry it is possible to resonantly couple the light corresponding to higher-order modes into the outer core, thus significantly increasing the leakage losses of the higher-order modes in comparison to the fundamental mode, thus making our proposed design to operate in an effectively single mode fashion with polarization independent propagation characteristics. The validation of the procedure is ensured with a detailed PBGF analysis based on an accurate finite element modal solver. Extensive numerical results show that the leakage losses of the higher-order modes can be enhanced in a level of at least 2 orders of magnitude in comparison to those of the fundamental mode. Our investigation is expected to remove an essential obstacle in the development of large-core single-mode hollow-core fibers, thus enabling them to surpass the attenuation of conventional fibers.



**OCIS codes:** (060.2280) Fiber design and fabrication; (060.2330) Fiber optics communications; (230.3990) Microstructure devices; (999.9999) Photonic crystal fiber.

## References and links

1. P. St. J. Russell, "Photonic crystal fibers," Science **299**, 358-362 (2003).
2. S. Kawanishi, T. Yamamoto, H. Kubota, M. Tanaka, and S. Yamaguchi, "Dispersion controlled and polarization maintaining photonic crystal fibers for high performance network systems," IEICE Trans. Electron. **E87-C**, 336-342 (2004).
3. R. F. Cregan, B. J. Mangan, J. C. Knight, T. A. Birks, P. St. J. Russell, P. J. Roberts, and D. C. Allan, "Single-mode photonic band gap guidance of light in air," Science **285**, 1537-1539 (1999).
4. P. Roberts, D. Williams, B. Mangan, H. Sabert, F. Couny, W. Wadsworth, T. Birks, J. Knight, and P. Russell, "Realizing low loss air core photonic crystal fibers by exploiting an antiresonant core surround," Opt. Express **13**, 8277-8285 (2005), http://www.opticsinfobase.org/abstract.cfm?URI=oe-13-20-8277.
5. G. Humbert, J. Knight, G. Bouwmans, P. Russell, D. Williams, P. Roberts, and B. Mangan, "Hollow core photonic crystal fibers for beam delivery," Opt. Express **12**, 1477-1484 (2004), http://www.opticsinfobase.org/abstract.cfm?URI=oe-12-8-1477.
6. J. Shephard, J. Jones, D. Hand, G. Bouwmans, J. Knight, P. Russell, and B. Mangan, "High energy nanosecond laser pulses delivered single-mode through hollow-core PBG fibers," Opt. Express **12**, 717-723 (2004), http://www.opticsinfobase.org/abstract.cfm?URI=oe-12-4-717.

7. T. Murao, K. Saitoh, and M. Koshiba, "Design of air-guiding modified honeycomb photonic band-gap fibers for effectively single mode operation," Opt. Express **14**, 2404-2412 (2006), http://www.opticsinfobase.org/abstract.cfm?URI=oe-14-6-2404 .
8. P. Roberts, F. Couny, H. Sabert, B. Mangan, D. Williams, L. Farr, M. Mason, A. Tomlinson, T. Birks, J. Knight, and P. St. J. Russell, "Ultimate low loss of hollow-core photonic crystal fibres," Opt. Express **13**, 236-244 (2005), http://www.opticsinfobase.org/abstract.cfm?URI=oe-13-1-236.
9. J. M. Fini. "Design of solid and microstructure fibers for suppression of higher order modes ," Opt. Express **13**, 3477-3490 (2005), http://www.opticsexpress.org/abstract.cfm?URI=OPEX-13-09-3477.
10. L. Lavoute, P. Roy, A. Desfarges-Berthelemot, V. Kermène, and S. Février, "Design of microstructured single-mode fiber combining large mode area and high rare earth ion concentration," Opt. Express **14**, 2994-2999 (2006), http://www.opticsinfobase.org/abstract.cfm?URI=oe-14-7-2994.
11. F. Gerome, J. L. Auguste, and J. M. Blondy. "Design of dispersion-compensating fibers based on a dual concentric-core photonic crystal fiber," Opt. Lett. **29**, 2725-2727 (2004).
12. K. Saitoh and M. Koshiba, "Leakage loss and group velocity dispersion in air-core photonic bandgap fibers," Opt. Express **11**, 3100-3109 (2003), http://www.opticsinfobase.org/abstract.cfm?URI=oe-11-23-3100.
13. K. Saitoh and M. Koshiba, "Full-vectorial imaginary-distance beam propagation method based on finite element scheme: Application to photonic crystal fibers," IEEE J. Quantum Electron. **38**, 927-933 (2002).
14. H. K. Kim, J. Shin, S. Fan, M. J. F. Digonnet, and G. S. Kino, "Designing air-core photonic bandgap fibers free of surface modes," IEEE J. Quantum Electron. **40**, 551-556 (2004).
15. C. M. Smith, N. Venkataraman, M. T. Gallagher, D. Müller, J. A. West, N. F. Borrelli, D. C. Allen, and K. W. Koch, "Low-loss hollow-core silica/air photonic band-gap fibre," Nature **424**, 657-659 (2003).
16. K. Saitoh and M. Koshiba, "Photonic bandgap fibers with high birefringence," IEEE Photon. Technol. Lett. **14**, 1291-1293 (2002).

## 1. Introduction

Microstructured optical fibers (MOFs) [1], also known as photonic crystal fibers (PCFs) or holey fibers (HFs), have stimulated much research and have shown great potentials in telecommunications and other applications [1, 2]. It has been conjectured that the light-wave guidance through air-cores via the photonic band gap (PBG) effect using a special category of MOFs known as photonic band gap fibers (PBGFs) [3], can revolutionize telecommunication industry, because light can be controlled in the fiber in ways not previously possible or even imaginable. This potential becomes clearer when the unique properties of PBGFs can be directly related to qualitatively new functionalities, or dramatic differences in performance. For example, the ability to guide light in a hollow-core suggests a new regime of transmission with ultra-low attenuation [4], and/or high power delivery with low nonlinearities [5, 6]. In addition, PBGFs may have more subtle but important advantages even when they behave more or less like conventional fibers.

One of the main drawbacks when guiding light through hollow-cores is the inevitable presence of higher-order modes (HOMs), which in the particular case of large cores they exhibit leakage losses sometimes comparable to those of the fundamental mode. Although suppression of HOMs can be observed in small-core PBGFs [7], there exist a fundamental limit of scattering losses due to the surface roughness scattering [8], which prohibits the further reduction of the fiber's attenuation to the level of the conventional fiber. One possible solution to overpass this limit is to consider large hollow-core PBGFs. Some intriguing designs have enhanced the suppression of HOMs [9] in index-guiding MOFs recently; however, extensive survey reveals that there is no any attempt in the international literature to design large effective mode area hollow-core PBGFs with suppressed HOMs for effectively single-mode operation.

In this paper, we show that the suppression of HOMs in hollow-core PBGFs can be successfully achieved through index-matching coupling between central core and outer core modes. This resonantly-matched mechanism has been observed previously in index-guiding MOFs [9]-[11].We take this intuitive mechanism and we propose a general methodology for designing PBGFs with suppressed HOMs. The basic design tradeoff between large effective mode areas and HOM suppression is explored for several structural parameters of PBGFs. We perform numerical simulations using an accurate and robust modal solver based on the finite element method (FEM) [12, 13], and we show that the presence of several hollow-cores in the

cladding of the PBGF, gives rise to resonant light-wave coupling between higher-order central core-modes and outer core-modes. This coupling was found to have a major impact in the enhancement of the leakage losses of HOMs. Extensive numerical results show that the leakage losses of the HOMs can be enhanced in a level of at least 2 orders of magnitude in comparison to those of the fundamental mode. The present investigation is expected to remove an essential obstacle in the development of large-core single-mode hollow-core PBGFs thus enabling them to surpass the attenuation of conventional fibers.

The present investigation is organized as follows: In Section 2 we introduce the basic design strategy for achieving the suppression of HOMs, by arranging several 7-unit-cell cores into the cladding of a PBGF with a 19-unit-cell central core, following a 6-fold symmetric pattern. Then in Section 3 we perform extensive numerical calculations, in order to identify the optimized structural parameters of the PBGF's profile, which will lead to the effectively single-mode operation. In Section 4 we briefly discuss the feasibility and the compatibility of the proposed design with other mature technologies. At last, in Section 5 we summarize our results and we give some concluded remarks and possible directions for future investigation.

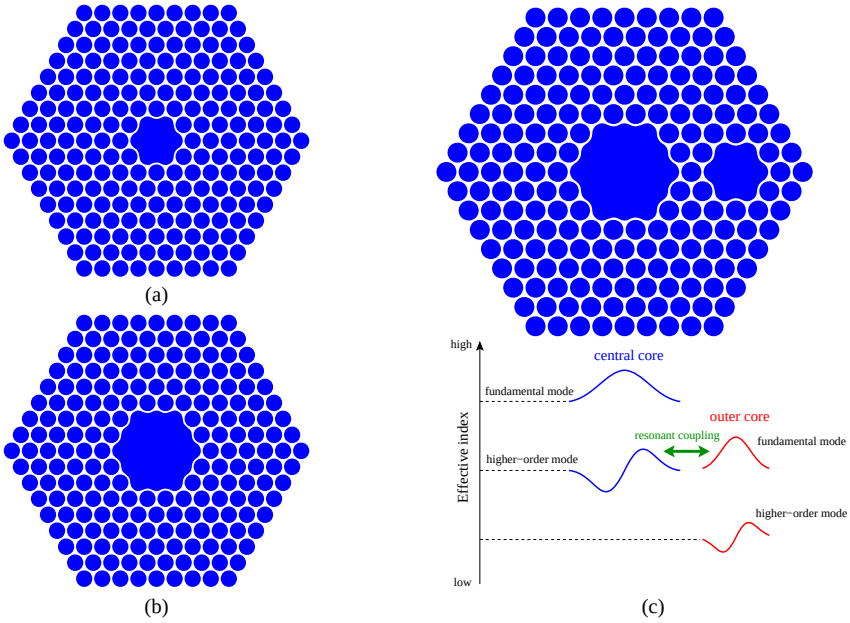


Fig.1. Schematic cross-sections of (a) a PBGF with a 7-unit-cell air-core, (b) a PBGF with a 19-unit-cell air-core, and (c) a non-standard PBGF with a 19-unit-cell central air-core and an additional 7-unit-cell outer core adjacent to the central core (upper panel). Blue and red curves (lower panel) show the field profiles of the fundamental and higher order modes for the central core and for the outer core, respectively, each corresponding to different effective indexes (left arrow). The presence of the outer core gives rise to resonant coupling between the central and outer core modes, suppressing in this way the existence of higher-order modes and permitting an effectively single-mode operation.

## 2. Design strategy for suppression of higher-order modes in large-hollow-core PBGFs

The design strategy for suppressing the HOMs by enhancing their attenuation is as follows: In Fig. 1(a) we can see the typical cross section of a standard 7-unit-cell hollow-core PBGF, where the core was created by removing two rings of tubes and smoothing the resulting core edges. Such PBGFs do not support surface modes, since the defected core surface does not intersect with the silica material where bulk mode has high intensity [14]. Although the 7-unit-cell hollow-core size is not so large, HOMs exist in it [15] and the difference between the

leakage losses of the HOMs and those of the fundamental mode is about one order of magnitude, and as a result it is difficult to realize low-loss single-mode operation using this structure. Recently, it has been reported that, in small core PBGFs with an optimized core and cladding profiles, the leakage losses of the HOMs are found to be at least three orders of magnitude larger than those of the fundamental mode [7]; however, the small core design makes it difficult to suppress the surface roughness scattering [8]. In order to form a large-core PBGF we can remove an additional air-hole ring and the resulting structure is depicted in Fig. 1(b). We will refer to this type of PBGF as a PBGF with a 19-unit-cell core. In order to enable the index matching mechanism to occur, we add a 7-unit-cell core adjacent to a 19-unit-cell central core, both integrated into the same fiber profile and the resulting structure can be seen in the upper panel of Fig. 1(c). In this case there is only one air-hole between the two adjacent cores; since we want a strong coupling to occur (such a strong coupling can not be achieved when using more periods to isolate the two cores). Typically, in a 19-unit-cell core PBGF we will have in total, two degenerated fundamental modes (denoted throughout the paper as $HE_{11}^{x}$ and $HE_{11}^{y}$ modes) [16], and four HOMs, two degenerated (denoted throughout the paper as $HE_{21}'$ and $HE_{21}''$ modes), and another two of $TE_{01}$-like and $TM_{01}$-like modes, where the terminology used to define the $TE_{01}$-like and $TM_{01}$-like modes has been depicted from the theory of conventional optical fibers. To visualize the co-existing fundamental modes in a 19-unit-cell core PBGF with structural parameters $d/\Lambda = 0.98$ and $\lambda/\Lambda = 0.5$, in Fig. 2 we plot the electric field vector distributions for the two degenerated fundamental modes, where $d$ is the diameter of the air holes, $\Lambda$ is the distance between adjacent air holes, and $\lambda$ is the operating wavelength. In particular Fig. 2(a) shows the vector field distribution of the $HE_{11}^{x}$ mode, and Fig. 2(b) shows the vector field distribution of the $HE_{11}^{y}$ mode. The qualitative visualization of the four HOMs is shown in Fig. 3, where in particular Fig. 3(a) shows the vector field distribution of the $HE_{21}'$ mode, Fig. 3(b) shows the vector field distribution of the $HE_{21}''$ mode, Fig. 3(c) shows the vector field distribution of the $TE_{01}$-like mode, and finally Fig. 3(d) shows the vector field distribution of the $TM_{01}$-like mode. The leakage losses of the HOM (in this case the $TE_{01}$-like mode) are almost the same as those of the fundamental mode, as will be demonstrated quantitatively later on.

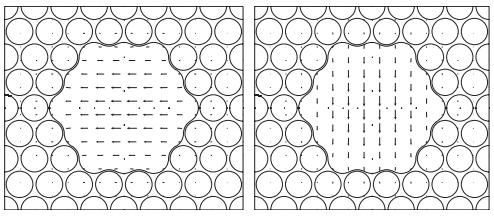

(a) (b)

Fig. 2. Electric field vector distributions of the two degenerated fundamental modes, (a) $HE_{11}^{x}$ and (b) $HE_{11}^{y}$ modes in a PBGF with 19-unit-cell core, and structural parameters of $d/\Lambda = 0.98$ and $\lambda/\Lambda = 0.5$.

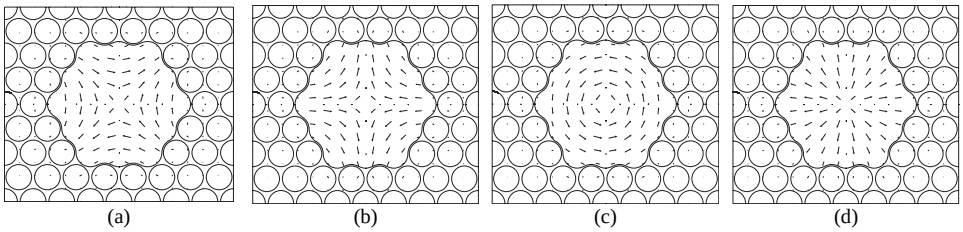

(a) (b) (c) (d)

Fig. 3. Electric field vector distributions of the four higher-order modes which are (a) $HE_{21}'$, (b) $HE_{21}''$, (c) $TE_{01}$-like, and (d) $TM_{01}$-like modes in a PBGF with 19-unit-cell core, and structural parameters of $d/\Lambda = 0.98$ and $\lambda/\Lambda = 0.5$.

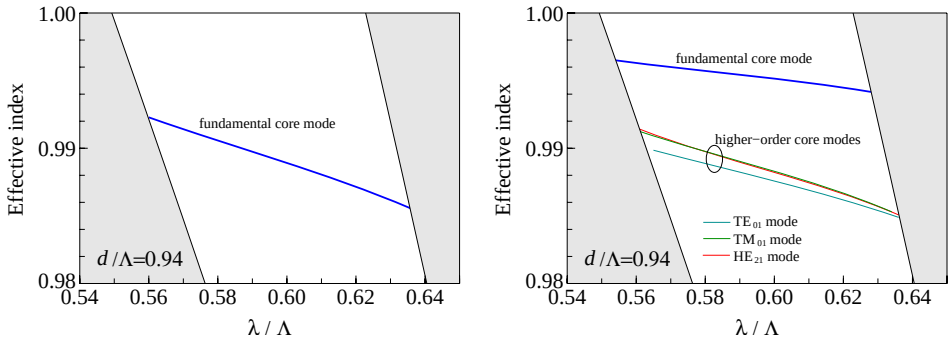


Fig. 4. Effective index curves as a function of the normalized wavelength λ/Λ for (a) a PBGF with 7-unit-cell core and (b) a PBGF with 19-unit-cell core, where $d/\Lambda$ = 0.94 and the grey strips represent the PBG boundaries.

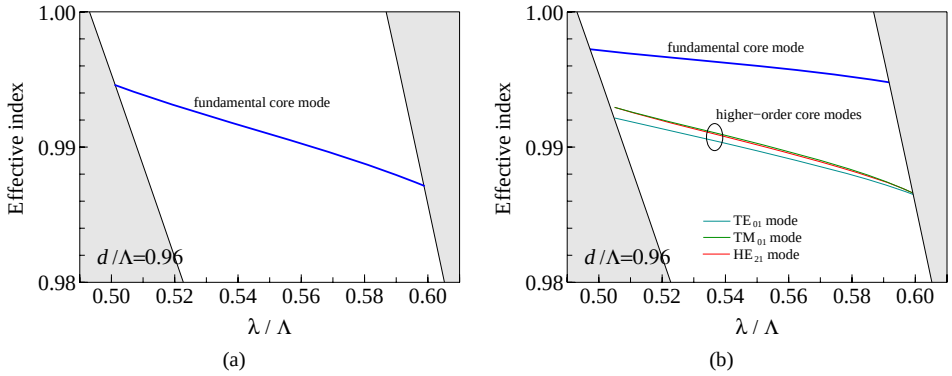


Fig. 5. Effective index curves as a function of the normalized wavelength λ/Λ for (a) a PBGF with 7-unit-cell core and (b) a PBGF with 19-unit-cell core, where $d/\Lambda$ = 0.96 and the grey strips represent the PBG boundaries.

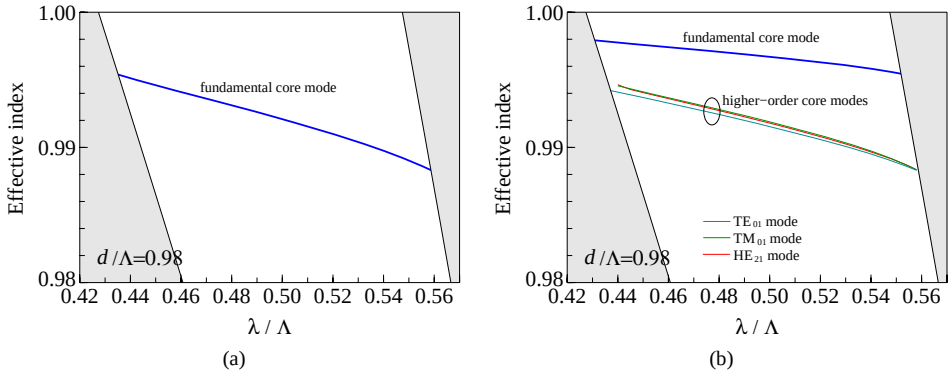


Fig. 6. Effective index curves as a function of the normalized wavelength λ/Λ for (a) a PBGF with 7-unit-cell core and (b) a PBGF with 19-unit-cell core, where $d/\Lambda$ = 0.98 and the grey strips represent the PBG boundaries.

The index matching mechanism we can achieve in our model can be explained through the knowledge of the effective refractive indexes. For the structures in Figs. 1(a) and (b), we calculate the effective refractive index curves as a function of the normalized wavelength $\lambda/\Lambda$ and for various structural parameters in Fig. 4 through Fig. 6, by using a full-vector FEM modal solver [12], where the refractive indices of air and silica are 1.0 and 1.45, respectively, and the shaded regions in Figs. 4-6 represent PBG boundaries calculated also by using FEM. In particular, Fig. 4 shows the computed effective refractive index of (a) the fundamental mode (blue curve) in a 7-unit-cell hollow-core PBGF and (b) the fundamental mode (blue curve) in a 19-unit-cell hollow-core PBGF as well as the three HOMs (since $HE_{21}'$ and $HE_{21}''$ modes are degenerated), that is $TE_{01}$-like mode (cyan curve), $TM_{01}$-like mode (green curve), and the degenerated $HE_{21}$ mode (red curve), for normalized air-hole diameters $d/\Lambda = 0.94$. The same calculation is repeated in Fig. 5 but for normalized air-hole diameters $d/\Lambda = 0.96$, and in Fig. 6 for normalized air-hole diameters $d/\Lambda = 0.98$. We have also confirmed the existence of additional higher order modes (the $EH_{11}$-like and $HE_{31}$-like modes), however their leakage losses are significantly larger that the first higher order modes, so we do not need to try to enhance further their leakage losses. From these results we may conclude that the obvious polarization dependence of the HOMs can be reduced by enlarging the air-hole size. From the results in Fig. 4 through Fig. 6 we can clearly see that the curve corresponding to the fundamental mode in the small-core PBGF is quite close to the curves corresponding to the effective refractive indices of the HOMs in the large-core PBGF. This fact can enable the index-matching mechanism to take place by bringing the two cores (large-central-core and outer-core) close to each other, thus enabling resonant coupling over a certain wavelength regime. The phenomenon is expected to be enhanced further, while keeping the polarization independent operation, if we place more outer-cores in the cladding by keeping the 6-fold symmetry around the central-core of the PBGF.

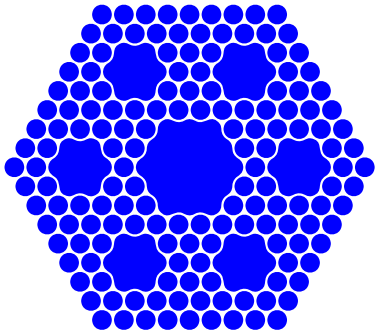

Fig. 7. Schematic cross-section of the proposed large-hollow-core PBGF profile with a 6-fold symmetric distribution of outer cores in the cladding. The index-matching mechanism can enable the resonant coupling of the higher-order modes of the central-core to the outer cores. By a judicious choice of the design parameters, this mechanism is expected to enhance the leakage losses of the higher-order modes, thus enabling effectively single-mode operation.

### 3. Derivation of the optimized structural parameters

Taking into account the index matching mechanism that can be obtained in the configuration of Fig. 1(c), we proceed by incorporating several 7-unit-cell cores into the cladding, surrounding the central core. The distribution of the outer cores follows a 6-fold symmetry because in such ideal system one expects polarization independent operation. The task is to find the appropriate design parameters of the resulting structure in Fig. 7 that would lead in the optimum enhancement of the leakage losses of the HOMs in comparison to the fundamental mode. In such optimized structure, although HOMs still exist, we can talk for an effectively single-mode operation over a certain wavelength window.

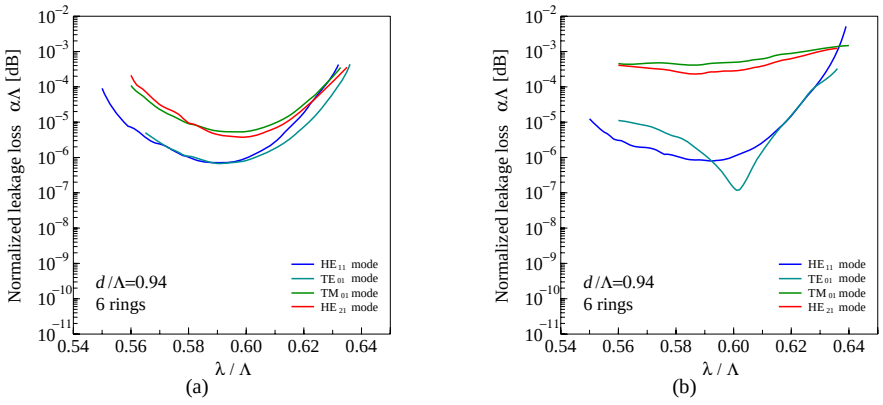


Fig. 8. Leakage loss properties as a function of the normalized wavelength for PBGF with a 19-unit-cell central core (a) without defected outer cores and (b) with defected outer cores, where $d/\Lambda$ = 0.94 and the number of air-hole ring is 6.

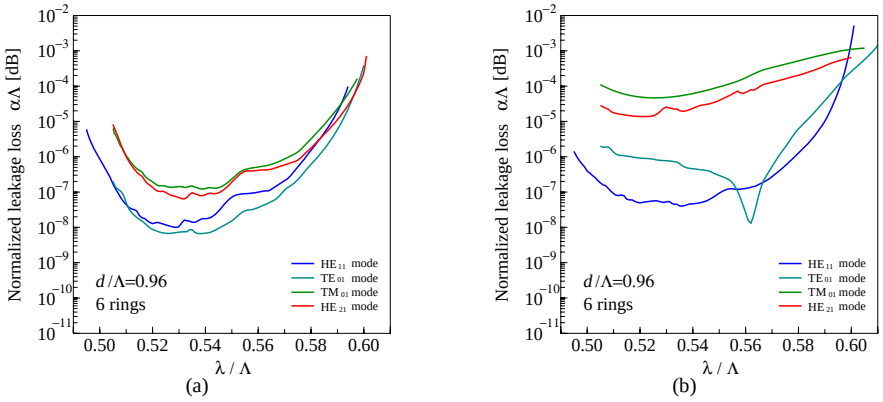


Fig. 9. Leakage loss properties as a function of the normalized wavelength for PBGF with a 19-unit-cell central core (a) without defected outer cores and (b) with defected outer cores, where $d/\Lambda$ = 0.96 and the number of air-hole ring is 6.

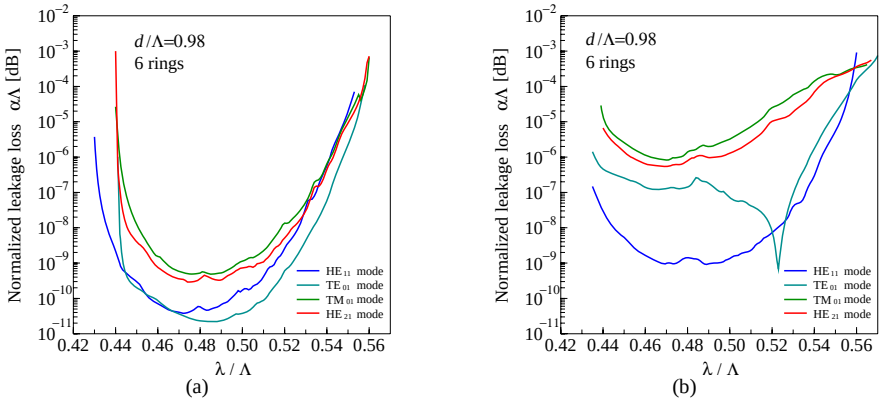


Fig. 10. Leakage loss properties as a function of the normalized wavelength for PBGF with a 19-unit-cell central core (a) without defected outer cores and (b) with defected outer cores, where $d/\Lambda$ = 0.98 and the number of air-hole ring is 6.

The normalized leakage loss properties $\alpha\Lambda$ in dB [12], as a function of the normalized wavelength $\lambda/\Lambda$ of the structure in Fig. 7 for several design parameters are shown in Fig. 8 through Fig. 10. In particular Fig. 8 shows the evaluation of the leakage losses for (a) the original 19-unit-cell core PBGF without defected cores, and (b) with defected cores in the cladding. The various curves correspond to different modes, namely the fundamental $HE_{11}$ mode (blue curves), the higher-order $TE_{01}$-like mode (cyan curves), the higher-order $TM_{01}$-like mode (green curves), and the degenerated higher-order $HE_{21}$-like mode (red curves). The computation has been performed for the following set of design parameters: $d/\Lambda = 0.94$, with the total number of the air-hole rings counted from the edge of the central core to the most outer air-hole ring is 6. The same evaluation of the normalized leakage loss properties is repeated in Fig. 9 for $d/\Lambda = 0.96$, and in Fig. 10 for $d/\Lambda = 0.98$, while keeping the total number of air-hole rings equal to 6. Regarding the leakage losses for the structure without defected cores in the cladding, we can clearly observe that the leakage losses corresponding to the higher-order $TE_{01}$-like mode (cyan curve) are comparable to those of the fundamental $HE_{11}$ mode (blue curve). On the other hand, the action of incorporating the outer cores into the fiber's profile has a major impact in the normalized leakage loss profile of the HOMs, especially we can see that the leakage losses of the $TM_{01}$-like mode (green curve), and the degenerated higher-order $HE_{21}$-like mode (red curve) can be enhanced significantly. As a conclusion there is a strong polarization dependent enhancement of the leakage losses of the HOMs in Fig. 8(b). On the other hand we can observe that by increasing the air-hole size $d/\Lambda$, the leakage loss of the $TE_{01}$-like mode (cyan curve) can be enhanced compared to the leakage loss of the fundamental $HE_{11}$ mode (blue curve), over a certain wavelength window. In addition we can see that regarding the leakage losses of the $TE_{01}$-like mode (cyan curve), there exist a deep peak in the corresponding curve which shifts to lower frequencies as soon as the air-hole size increases. The physical explanation of this global extreme peak is as follows: At first it was observed that the effective index difference between the $TE_{01}$-like mode (cyan curve) in the 19-unit-cell core and the fundamental $HE_{11}$ mode (blue curve) in the 7-unit-cell-core is larger than the corresponding index difference of all the other higher-order modes ($TM_{01}$-like mode and $HE_{21}$-like modes). Secondly it was found that the effective mode area corresponding to the $TE_{01}$-like mode in the 19-unit-cell core is smaller than the corresponding effective mode area of all the other higher-order modes and decreases as the operational wavelength increases. These two facts explain the continuous decrement of the leakage loss property of the $TE_{01}$-like mode. When the global minimum has reached, then due to the existence of the PBG-edge in the upper wavelength range, the leakage loss is forced to increase. We can clearly see that this peak becomes sharper when the normalized air-hole diameter $d/\Lambda$ increases. From the results depicted in Fig. 8 through Fig. 10 we can conclude that the enhancement of the leakage losses of HOMs comes from the strong coupling between the central large core and the adjacent outer cores. The optimization of this enhancement can be solely controlled by adjusting only a single design parameter, which is the size of the air-holes $d/\Lambda$ in the fiber's profile.

The propagation properties of the de-normalized structure that exhibits optical functionality in the telecommunication window are quantitatively shown in Fig. 11. Optimized structural parameters were chosen based on the previous observations as: $d/\Lambda = 0.98$ and $\Lambda = 3.23$ μm, while the total number of the air-hole rings counted from the edge of the central core to the most outer air-hole ring is 6. For this fiber's profile, Fig. 11(a) shows the computed effective refractive index curves of the fundamental $HE_{11}$ mode (blue curve), the higher-order $TE_{01}$-like mode (cyan curve), the higher-order $TM_{01}$-like mode (green curve), and the degenerated higher-order $HE_{21}$-like mode (red curve), as a function of the operational wavelength. In Fig. 11(b) we compute the leakage losses in dB/km of the fundamental $HE_{11}$ mode (blue curve), the higher-order $TE_{01}$-like mode (cyan curve), the higher-order $TM_{01}$-like mode (green curve), and the degenerated higher-order $HE_{21}$-like mode (red curve), as a function of the operational wavelength. From these results we find that the optimized structure

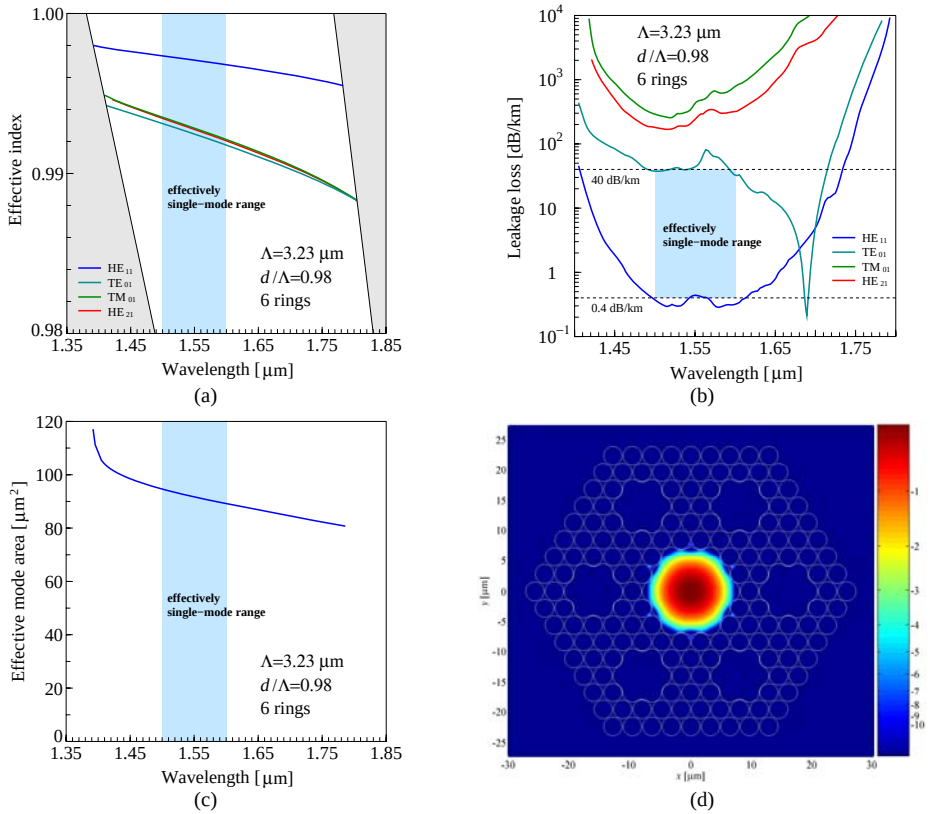


Fig. 11. (a) Effective index curves as a function of the operational wavelength for the fundamental $HE_{11}$ mode (blue curve), the higher-order $TE_{01}$-like mode (cyan curve), the higher-order $TM_{01}$-like mode (green curve), and the degenerated higher-order $HE_{21}$mode (red curve), with the PBG boundaries denoted with the grey strips, (b) leakage loss properties of the modes for the optimized structure as a function of the operational wavelength, (c) the effective mode area as a function of the wavelength, and (d) the electric field distribution of the fundamental $HE_{11}$ mode at a wavelength of $\lambda$ = 1.55 μm. In all cases above the effectively single-mode operational bandwidth is denoted as a cyan strip.

exhibits an effectively single-mode operation from 1.5 μm to 1.6 μm wavelength range (namely over a 100 nm bandwidth), with the leakage loss level of the fundamental $HE_{11}$ mode (blue curve) to remain below 0.4 dB/km, while the leakage loss level of the higher-order $TE_{01}$-like mode (cyan curve) to remain above 40 dB/km. So the leakage loss of the $TE_{01}$-like mode has been enhanced about 2 orders of magnitude over a 100 nm wavelength window. To ensure that the optimized structure of Fig. 7 can be successfully used as a data transmission platform, a very crucial quantity in terms of the quality of the information transmission is the available effective mode area of the structure. The effective mode area for the optimized structure is shown in Fig. 11(c) as a function of the operational wavelength. The effective mode area of the fiber core, $A_{eff}$, is defined as:

$$A_{eff} = \frac{\left(\iint |\boldsymbol{E}|^2 dxdy\right)^2}{\iint |\boldsymbol{E}|^4 dxdy}, \tag{1}$$

where $\boldsymbol{E}$ is the electric field vector. From this graph we can fairly conclude that the effective mode area stays above 89 $\mu m^2$ from 1.5 μm to 1.6 μm wavelength range. The effective mode

area in this case is at the same level as that of a conventional single-mode fiber (SMF), thus enabling the potential use of the proposed structure as a platform for information transmission with low losses and low nonlinearities. In order to visualize the light-wave confinement in the optimized structure, in Fig. 11(d), we plot the electric field distribution ($E_x$) of the *x*-polarized fundamental $HE_{11}$ mode at a wavelength of $\lambda$ = 1.55 μm. It is evident that the mode is confined nicely into the core of the fiber with corresponding effective mode area of about 92 $\mu m^2$.

In order to visualize the index-matching phenomenon which gives rise to strong coupling of the HOMs from the central core to the outer cores, which is responsible for the effectively single-mode operation of the proposed structure, in Fig. 12 we plot the field distributions of the higher-order $TM_{01}$-like mode at a wavelength of $\lambda$ = 1.7 μm. The choice of this particular wavelength was done because there is strong coupling of the HOM into the outer cores for better visualization of the modal profiles. In particular Fig. 12(a) shows the *x*-component of the electric field distribution of the higher-order $TM_{01}$-like mode at a wavelength of $\lambda$ = 1.7 μm, while Fig. 12(b) shows the *y*-component of the electric field distribution of the higher order $TM_{01}$-like mode at the same wavelength. The main conclusion in both cases is that there is an obvious coupling of the HOM into the outer cores. On the other hand in the absence of defected outer cores no such coupling occurs and the HOM is confined into the central core as can be seen clearly in Fig. 12(c) for the *x*-component of the electric field, and in Fig. 12(d) for the *y*-component of the electric field.

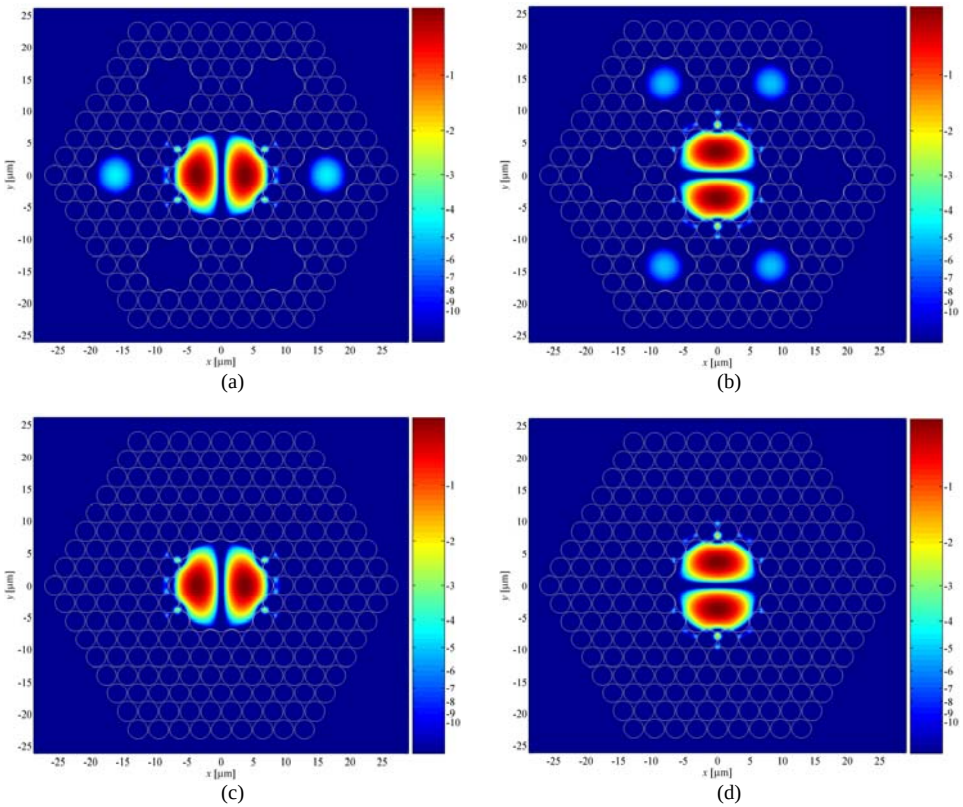


Fig. 12. Visualization of the electric field distributions in dB of the higher-order $TM_{01}$-like mode at a wavelength of $\lambda$ = 1.7 μm, in the presence of outer cores for (a) *x*-component of the electric field, and (b) *y*-component of the electric field, and in the absence of outer cores for (c) *x*-component of the electric field and (d) *y*-component of the electric field. Notice the strong coupling of the higher-order mode to the outer cores in the first two cases.

## 4. Feasibility and compatibility of the proposed large-hollow-core PBGF

Although the objective of the present investigation was the theoretical description of the index matching mechanism as ingredient for the effective enhancement of the leakage losses of the HOMs in large-hollow-core PBGFs, and the experimental verification of our results remains to be performed, at this point, we wish to address some possible drawbacks regarding the feasibility and the compatibility of our proposed structure with other conventional fiber architectures. At first, we should point out that our structure exhibits a perfect 6-fold symmetry. In practical realization of such a structure however, such perfect 6-fold symmetry will be difficult to keep. In such a situation, it is expected that the leakage losses for each polarization of the HOMs would slightly change; however, the single-mode operation based on the principle of index-matching mechanism will still operate effectively. Possible structural disorders and/or core deformation may be possible and we are expecting in such realistic scenario that the difference of the leakage losses between fundamental and HOMs would slightly decrease. Regarding the investigated core-shapes, it may be difficult to realize them using the current fabrication technologies. In such realistic situation, surface modes may exist, and if they lie within the effectively single-mode region of the fiber, we expect that the bandwidth of the effectively single-mode region will be reduced. Regarding the PBGF with a 7-unit-cell hollow-core, it is difficult to splice with a conventional SMF due to the mode field diameter mismatch between the SMF and the PBGF in the telecommunication band. On the other hand, since the effective mode area of a PBGF with a 19-unit-cell hollow-core is comparable to that of a conventional SMF, we would expect low-loss splicing between the SMF and the proposed large-hollow-core PBGF.

## 5. Conclusions

To conclude the present investigation, we have described a thorough methodology for suppressing the HOMs in large-hollow-core PBGFs, thus permitting an effectively single-mode operation. Our proposed method relies on the existence of several 7-unit-cell cores into the cladding of PBGF with a 19-unit-cell hollow-core, following a 6-fold symmetric pattern. The optimization of the proposed structure was achieved by presenting numerical results for various design parameters using a rigorous computational tool based on the finite element computational scheme. Our proposed structure exhibits the following propagation characteristics: effectively single-mode operation from 1.5 μm to 1.6 μm wavelength range with the leakage losses of the HOMs to be enhanced at least 2 orders of magnitude (40 dB/km) in comparison to those of the fundamental mode (0.4 dB/km), and an effective mode area of about 90 $\mu m^2$, which is comparable to that of a conventional SMF. Further optimization of the device may be possible and is currently under investigation. The main conclusion is that the optimized structure can easily meet all the requirements for single-mode operation in typical transmission platforms. It is expected that the experimental realization of the proposed structure will open new possibilities for light-wave guidance in hollow-cores, and further suggest a new regime of transmission with ultra-low attenuations and/or high power delivery with ultra-low nonlinearities. The inclusion of deformed shapes in the cladding of PBGFs is an interesting research topic with many intriguing applications.

## Acknowledgements

K. Saitoh acknowledges stimulating discussions with Dr. John M. Fini from OFS Laboratories.